

A COMPARISON OF MULTIPLICITY DISTRIBUTIONS AND TWO-PARTICLE  
RAPIDITY CORRELATIONS IN ANTIQUARK-PROTON AND PROTON-PROTON  
INTERACTIONS AT THE CERN-ISR

CERN-Napoli-Pisa-Stony Brook Collaboration<sup>\*)</sup>

*Presented by V. Cavasinni<sup>\*\*)</sup>*  
INFN and Scuola Normale Superiore, Pisa, Italy



ABSTRACT

We have investigated the properties of topological cross-sections and particle correlations in antiproton-proton and proton-proton collisions at the CERN ISR. The distribution of the  $\bar{p}p$ -pp difference in topological cross-sections has a shape and energy dependence markedly different from the pp or  $\bar{p}p$  distributions. Instead it is found to be similar to the multiplicity distributions found in very inelastic processes, such as  $e^+e^-$  annihilation into hadrons. A direct comparison of two-body rapidity correlations in  $\bar{p}p$  and pp interactions shows that, in the  $\bar{p}p$  case, there is, superimposed on the usual short-range correlation, a correlation of very short range. A simple quark-antiquark annihilation model is proposed to explain this effect.

<sup>\*)</sup> M. Ambrosio, G. Anzivino, G. Barbarino, G. Carboni, V. Cavasinni, T. Del Prete, D. Lloyd Owen, M. Morganti, G. Paternoster, S. Patricelli, F. Schiavo, and M. Valdata-Nappi.

<sup>\*\*)</sup>  Visitor at CERN.

1. INTRODUCTION

The measurement of total cross-sections in  $\bar{p}p$  and  $pp$  collisions at the ISR<sup>1-3)</sup> demonstrated that differences between antiproton-proton and proton-proton interactions -- while diminishing -- are still appreciable at high energy. In particular, at  $\sqrt{s} = 31$  GeV,  $\sigma_{\bar{p}p} - \sigma_{pp} = 2.3 \pm 0.3$  mb<sup>4)</sup>, and almost the entire difference can be ascribed to the inelastic part of the total cross-sections. The extra number of inelastic events, which contribute only in the  $\bar{p}p$  channel, could have topological characteristics different from the soft "peripheral" events common to both  $\bar{p}p$  and  $pp$  interactions. These effects have already been studied at  $\sqrt{s} = 13.8$  GeV<sup>5)</sup>; the results of this investigation show that the differences of inelastic topological cross-sections  $\sigma(\bar{p}p) - \sigma_n(pp)$  have moments which differ from those of  $\sigma_n(pp)$  [or  $\sigma_n(\bar{p}p)$ ] and are in agreement with the trend observed in the  $\bar{p}p$  annihilation channel, directly measured only at very low energy.

In this paper we wish to draw attention to the difference in topological cross-sections (also called the annihilation multiplicity distribution) and to a comparison of two-particle rapidity correlations in the two processes. The latter quantity measures the level of clustering of the final-state particles and, as we shall see, sheds light on the origin of the persisting  $\bar{p}p/pp$  differences.

2. THE EXPERIMENT

The apparatus which is the same as that used for the measurement of the total cross-section, has been described in detail elsewhere<sup>1,2)</sup>. Briefly, it consists of a set of drift chambers detecting particles in a pseudorapidity interval  $|\eta| < 2$  with good  $\eta$  resolution (as good as 0.05 in the central  $\eta$  region), and a system of scintillation-counter hodoscopes with a larger  $\eta$  coverage ( $|\eta| \leq 5$ ) but -- owing to the finite size of the counters -- poorer  $\eta$  resolution. The trigger of the experiment is provided by coincidences of pairs of hodoscope planes positioned on the left and right sides of the intersection<sup>1,2)</sup> and, in the configuration employed for this analysis, it was sensitive to about 90% of all inelastic events. The off-line analysis imposes the existence of a primary vertex reconstructed by the chamber system with at least two tracks emitted within  $|\eta| < 2^*$ <sup>3)</sup>. The event multiplicity was computed as the sum of reconstructed tracks and hits in the non-overlapping counters outside the region covered by the chamber system.

The data have not been corrected for secondary interactions,  $\delta$ -rays, binning effects, etc. As a result, our raw  $pp$  average multiplicity is proportional to the value already published<sup>5)</sup> with a proportionality factor  $K$ , which is independent of energy.

<sup>\*)</sup> This requirement eliminates any contributions from diffractive events, but still includes about 70% of all inelastic interactions.

### 3. THE RESULTS

Figure 1 shows the topological cross-sections at  $\sqrt{s} = 31$  GeV for  $\bar{p}p$  and  $pp$  interactions: the two distributions appear quite similar, the relative difference of the mean values being  $(\langle n \rangle_{pp} - \langle n \rangle_{\bar{p}p}) / \langle n \rangle_{pp} = 0.02 \pm 0.01$ . The ratio  $\langle n \rangle / D = 2.01 \pm 0.1$  for the two reactions in good agreement with the data of Thomé et al.<sup>6</sup>). Figure 2 shows the difference in topological cross-sections at a)  $\sqrt{s} = 31$  GeV, b)  $\sqrt{s} = 53$  GeV, and c)  $\sqrt{s} = 63$  GeV. From Fig. 2 one sees that the mean values of the annihilation multiplicity distributions are larger than those in  $pp$  distributions by a factor of  $1.3 \pm 0.1$  at  $\sqrt{s} = 31$  and 53 GeV, and 1.5 at  $\sqrt{s} = 63$  GeV.

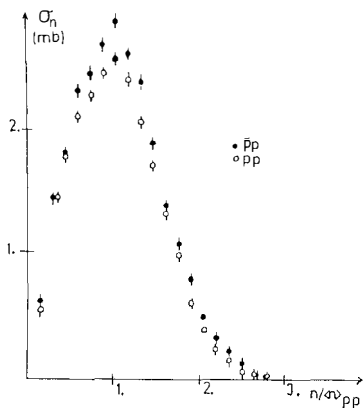


Fig. 1 Topological cross-sections in  $\bar{p}p$  and  $pp$  interactions at  $\sqrt{s} = 31$  GeV plotted as a function of the charged multiplicity normalized to the average  $pp$  multiplicity.

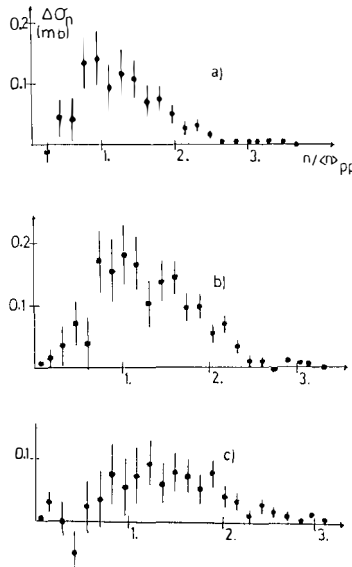


Fig. 2 The  $\bar{p}p$ - $pp$  difference in topological cross-sections at a)  $\sqrt{s} = 31$  GeV, b)  $\sqrt{s} = 53$  GeV, and c)  $\sqrt{s} = 63$  GeV versus the normalized charged multiplicity  $n_{ch}/\langle n \rangle_{pp}$ .

Figure 3 shows the  $\bar{p}p$  and  $pp$  multiplicity distributions and the annihilation multiplicity distribution at  $\sqrt{s} = 31$  GeV plotted in KNO scaling variables<sup>7</sup>). Again one sees little difference between  $\bar{p}p$  and  $pp$ : both distributions agree reasonably well with the Slattery parametrization<sup>8</sup>) (solid line in the figure). The annihilation distribution is, instead, narrower than that for  $\bar{p}p$  or  $pp$ , its shape being in better agreement with the broken curve, which is a fit to lower-energy annihilation data<sup>9</sup>) and also reproduces rather well the hadronic multiplicity distribution measured in  $e^+e^-$  annihilations at PETRA<sup>10</sup>).

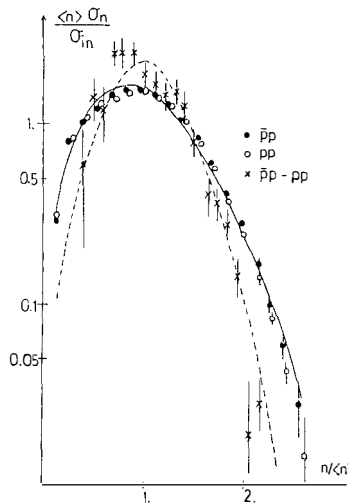


Fig. 3 KNO multiplicity distribution at  $\sqrt{s} = 31$  GeV for  $\bar{p}p$ ,  $pp$ , and  $\bar{p}p - pp$ . The solid line is a fit to the  $pp$  data in the range 50-303 GeV/c of incident momentum<sup>8</sup>). The broken curve is a fit of low-energy  $\bar{p}p$  annihilation data<sup>9</sup>.

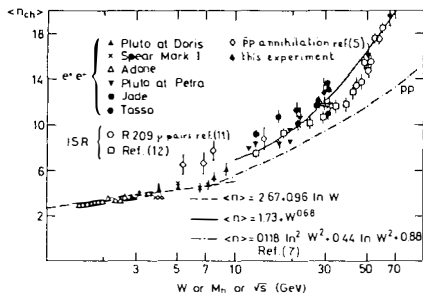


Fig. 4 Comparison of energy dependence of mean annihilation multiplicities observed in this experiment with the values measured in low-energy  $\bar{p}p$  annihilations<sup>5</sup>),  $e^+e^-$  hadronic annihilation<sup>10</sup>),  $\mu$ -pair events<sup>11</sup>),  $pp$  interactions with leading particles subtracted<sup>12</sup>).

The common features of  $e^+e^-$  and  $\bar{p}p$ - $pp$  annihilation processes lead one to compare the energy dependence of the multiplicities in the two processes. To accomplish this, our raw annihilation multiplicities were corrected by the factor  $K$ , previously discussed, which corrects globally for secondary interactions, binning effects, etc. Figure 4 shows our annihilation values compared with multiplicities measured in other very inelastic interactions; we see that our points are in good agreement with the QCD curve fitting the energy dependence of the  $e^+e^-$  data at high energy, which are, in turn, in agreement with hadron multiplicities measured in other very inelastic processes, such as lower-energy  $\bar{p}p$  annihilation<sup>5</sup>),  $\mu$ -pair events<sup>11</sup>), and  $pp$  interactions where the leading-particles have been removed<sup>12</sup>).

The pseudorapidity correlation function obtained after integrating over azimuth is defined by the following expression:

$$R_2(\eta_1, \eta_2) = \frac{\rho_2(\eta_1, \eta_2)}{\rho_1(\eta_1)\rho_1(\eta_2)} - 1 ,$$

where  $\rho_2(\eta_1, \eta_2)$  is the two-particle density at  $(\eta_1, \eta_2)$  and  $\rho(\eta)$  is the single-particle density at  $\eta$ . If particles are emitted independently  $R_2(\eta_1, \eta_2)$  is zero.

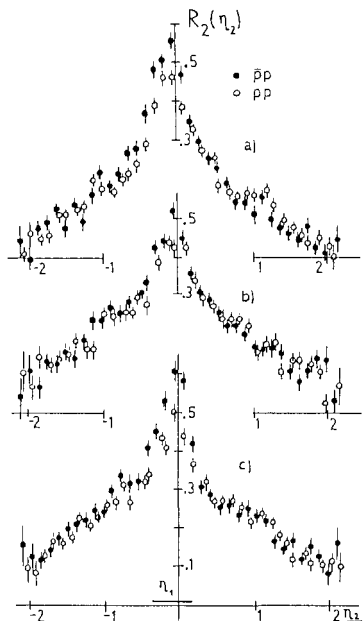


Fig. 5  $R_2(\eta_1, \eta_2)$  vs  $\eta_2$  for fixed  $\eta_1$  in  $\bar{p}p$  and  $p\bar{p}$  interactions at c.m. energies of  
a) 31 GeV, b) 53 GeV, and c) 63 GeV.

Figure 5 shows  $R_2(\eta_1, \eta_2)$  as a function of  $\eta_2$  for  $\bar{p}p$  and  $p\bar{p}$  collisions at the three energies: a) 31 GeV, b) 53 GeV, and c) 63 GeV. The correlation function has been integrated over the range  $-0.36 \leq \eta_1 \leq 0.12$ , and the bin width in  $\eta_2$  is  $\Delta\eta_2 = 0.12$  units. The most striking aspect of Fig. 5 is the extra component of correlation at the maxima of  $\bar{p}p$  distribution. This excess of correlation is limited to a range in  $\eta_2$  of about  $\pm 0.3$  units. Reducing by a factor of 2 the  $\eta_1$  interval over which  $R_2$  was integrated, we found no appreciable change in the width of the  $\bar{p}p$  excess in  $\eta_2$  -- it is much narrower than the short-range correlations common to both reactions and, consequently, is indicative of a separate dynamical mechanism.

To investigate the dependence of the correlation in two dimensions rather than one, we calculated  $R_2(\eta_1, \eta_2)$  for a number of values of fixed  $\eta_1$ . The results are shown in Fig. 6 for six  $\eta_1$  intervals at  $\sqrt{s} = 31$  GeV<sup>\*)</sup>. Both  $\bar{p}p$  and  $p\bar{p}$  correlation functions have maxima at  $\eta_1 = \eta_2$ , as expected from earlier correlation studies<sup>1,3</sup>. The  $\bar{p}p$  excess, however, diminished as  $\eta_1$  moves away from zero. In order to quantify the dependence of the extra  $\bar{p}p$  correlation, we integrated the difference  $\Delta R_2 = R_2(\bar{p}p) - R_2(p\bar{p})$  over  $\eta_2$  at each  $\eta_1$  setting and plotted this difference as a function of  $\eta_1$ . The results are shown in Fig. 7. One sees clearly that the enhancement of the  $\bar{p}p$  correlation function occurs only for  $-1 < \eta_1 \approx \eta_2 < 1$ .

\*) In the following we shall discuss only data at  $\sqrt{s} = 31$  GeV. We checked that the other energies also show similar features.

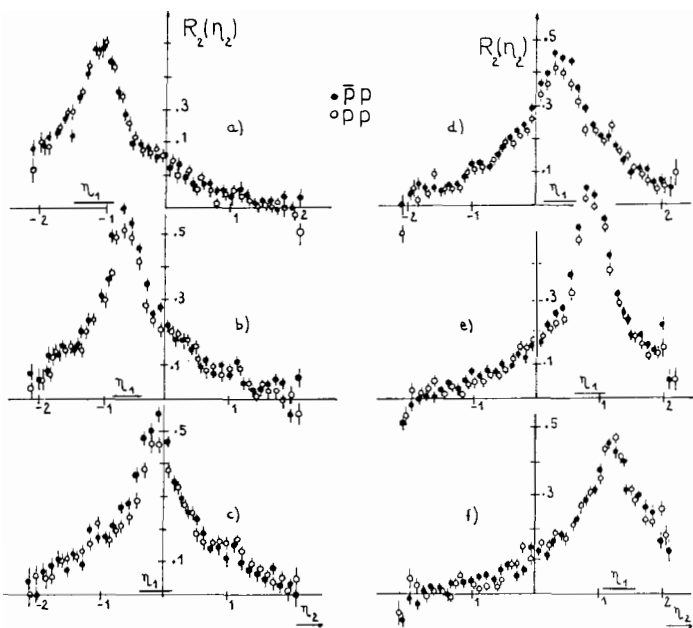


Fig. 6  $R_2(n_1, n_2)$  in  $\bar{p}p$  and  $p p$  interactions at 31 GeV as a function of  $n_2$  for six regions of fixed  $n_1$ .

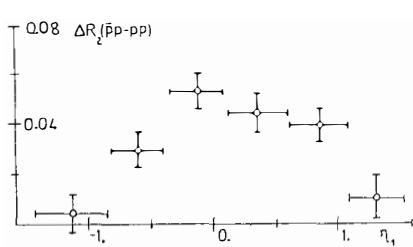
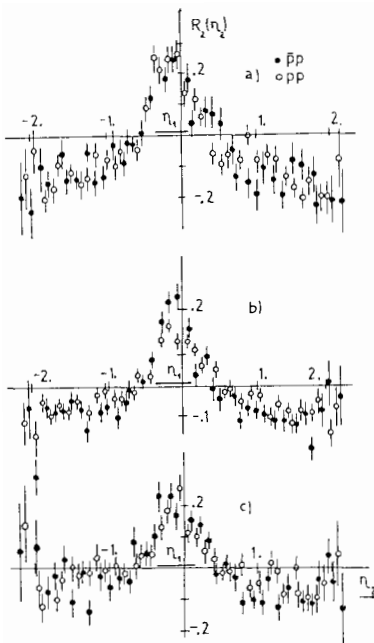


Fig. 7 The  $\bar{p}p$ - $p p$  difference in  $R_2(n_1, n_2)$  integrated over  $n_2$  as a function of  $n_1$  at  $\sqrt{s} = 31$  GeV.

Fig. 8 The semi-inclusive correlation function in  $\bar{p}p$  and  $p p$  interactions at  $\sqrt{s} = 31$  GeV for a)  $n_{ch} < \frac{2}{3}\langle n \rangle_{ann}$ , b)  $\frac{2}{3}\langle n \rangle_{ann} < n_{ch} < \frac{4}{3}\langle n \rangle_{ann}$ , c)  $n_{ch} > \frac{4}{3}\langle n \rangle_{ann}$ .



We then investigated the correlation semi-inclusively, i.e. in different multiplicity ranges. Figure 8 shows this study for three multiplicity ranges: a) lower than the average annihilation multiplicity, b) around the average, and c) greater than the average. The  $\bar{p}p$  enhancement is clearly visible only in the middle range, where, in fact, the differences in the  $\bar{p}p$  and  $p\bar{p}$  topological cross-sections are larger.

In the framework of quantum chromodynamics (QCD), one might expect that quark-antiquark annihilation into quark or gluon pairs would play a more important role in  $\bar{p}p$  collisions than it does in  $p\bar{p}$ , and, in that case, yield extra events in which two jets of particles are emitted. Owing to the balanced quark and antiquark structure functions in the proton and in the antiproton, this production would be central in rapidity. The collimation of the particles belonging to these jets could be the origin of the excess of correlation observed in  $\bar{p}p$  collisions. One expects the scattered quark and antiquark (in excess in the  $\bar{p}p$  case) to carry some GeV of transverse momentum; therefore they should fragment into few particles with opening angles of  $\sim 20^\circ$ , as do the jets observed at SPEAR and DORIS. At  $\eta = 0, 20^\circ$  of angular dispersion corresponds to a pseudorapidity width of about 0.3, as observed in our correlation data.

As a check of this hypothesis we have made a naive Monte Carlo calculation, in which two jets are superimposed on events from our  $p\bar{p}$  data with a variable frequency. The jets were generated with their axes at  $\eta = 0$ , back-to-back in azimuth, and with a mean multiplicity of  $\langle n \rangle_{jet} = 2$ . The dispersion of jet particles in rapidity was  $\Delta\eta = 0.3$ . The frequency  $x$  of generation was adjusted to reproduce the amount of the excess of correlation observed in the  $\bar{p}p$  data. The result of this calculation is shown in Fig. 9: the excess of  $\bar{p}p$  correlation is nicely reproduced with a jet superimposed once every 70 events (compared Fig. 9 with Fig. 5a).

We note also that the inelastic cross-sections measured for  $\bar{p}p$  and  $p\bar{p}$ , within the cuts imposed by the correlation analysis, are 16.2 and 18 mb, respectively, i.e. the difference of cross-section is  $\sim 10\%$  of the total  $p\bar{p}$  cross-section. Instead, the optimal frequency of generation in the Monte Carlo was only  $x = 1.4\%$ , which suggests that only a fraction of the difference in cross-section can be attributed to hard  $\bar{q}q$  annihilations.

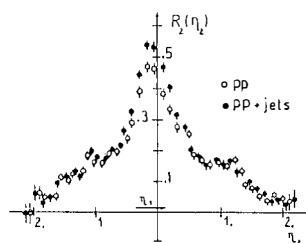


Fig. 9  $R_2(\eta_1, \eta_2)$  in  $p\bar{p}$  interactions at  $\sqrt{s} = 31$  GeV compared with the results of a Monte Carlo calculation incorporating the contribution of two jets (see text).

4. CONCLUSIONS

We can summarize this study of inelastic interactions in  $\bar{p}p$  and  $p\bar{p}$  collisions at the ISR energies as follows:

- i) The  $\bar{p}p$ - $p\bar{p}$  difference in topological cross-sections shows remarkable divergence from the unsubtracted  $\bar{p}p$  or  $p\bar{p}$  multiplicity distributions, resembling far more to the hadronic multiplicity distributions in  $e^+e^-$  annihilations (or other very inelastic reactions).
- ii) In  $\bar{p}p$  inelastic collisions, the particles produced are more correlated than in  $p\bar{p}$  interactions. This excess of correlations has a range in  $\eta$  of  $\sim 0.3$  and it is confined to the central  $\eta$  region,  $|\eta| < 1$ . A simple phenomenological model, in which a fraction (10-15%) of the difference between  $\bar{p}p$  and  $p\bar{p}$  inelastic cross-sections stems from hard  $\bar{q}q$  annihilation into two jets emitted centrally in  $\eta$ , could explain the excess of  $\bar{p}p$  correlations.

REFERENCES

- 1) G. Carboni et al., Phys. Lett. 108B, 145 (1982).
- 2) G. Carboni et al., Phys. Lett. 113B, 87 (1982).
- 3) N. Amos et al., Phys. Rev. Lett. 47, 1191 (1981).
- 4) T. Del Prete, these Proceedings.
- 5) J.G. Rushbrooke et al., Phys. Lett. 59B, 303 (1975).
- 6) W. Thomé et al., Nucl. Phys. B129, 365 (1977).
- 7) Z. Koba, H.B. Nielsen and P. Olesen, Nucl. Phys. B40, 317 (1972).
- 8) P. Slattery, Phys. Rev. D 7, 2073 (1973).
- 9) J. Salava and V. Simak, Nucl. Phys. B69, 15 (1973).
- 10) Ch. Berger et al., Phys. Lett. 95B, 313 (1980).
- 11) D. Antreasyan et al., Nucl. Phys. B199, 365 (1982).
- 12) M. Basile et al., Phys. Lett. 95B, 311 (1980).
- 13) See, for example, S.R. Amendolia et al., Phys. Lett. 48B, 359 (1974).